Environmental Science
Processes & Impacts

Accepted Manuscript

Biological versus Mineralogical Chromium Reduction: Potential for Reoxidation by Manganese Oxide

Elizabeth C. Butler[1*], Lixia Chen[1, 5], Colleen M. Hansel[2], Lee R. Krumholz[3], Andrew S. Elwood Madden[4], Ying Lan[1]

[1]School of Civil Engineering and Environmental Science, University of Oklahoma, Norman, OK 73019

[2]Department of Marine Chemistry and Geochemistry, Woods Hole Oceanographic Institution, Woods Hole, MA 02543

[3]Department of Microbiology and Plant Biology and Institute for Energy and the Environment, University of Oklahoma, Norman, OK 73019

[4]School of Geology and Geophysics, University of Oklahoma, Norman, OK 73019

[5]Present address: Oklahoma Department of Environmental Quality, Oklahoma City, OK 73102

Revised and resubmitted to *Environmental Science: Processes & Impacts*

September 30, 2015

*Corresponding author: phone: +1 405-325-3606; Fax: +1 405-325-4217; E-mail: ecbutler@ou.edu

Electronic Supplementary Information (ESI) available: Additional figures. See

DOI: 10.1039/x0xx00000x

Abstract

Hexavalent chromium (Cr(VI), present predominantly as CrO_4^{2-} in water at neutral pH) is a common ground water pollutant, and reductive immobilization is a frequent remediation alternative. The Cr(III) that forms upon microbial or abiotic reduction often co-precipitates with naturally present or added iron (Fe), and the stability of the resulting Fe-Cr precipitate is a function of its mineral properties. In this study, Fe-Cr solids were formed by microbial Cr(VI) reduction using *Desulfovibrio vulgaris* strain RCH1 in the presence of the Fe-bearing minerals hematite, aluminum substituted goethite (Al-goethite), and nontronite (NAu-2, Clay Minerals Society), or by abiotic Cr(VI) reduction by dithionite reduced NAu-2 or iron sulfide (FeS). The properties of the resulting Fe-Cr solids and their behavior upon exposure to the oxidant manganese (Mn) oxide (birnessite) differed significantly. In microcosms containing strain RCH1 and hematite or Al-goethite, there was significant initial loss of Cr(VI) in a pattern consistent with adsorption, and significant Cr(VI) was found in the resulting solids. The solid formed when Cr(VI) was reduced by FeS contained a high proportion of Cr(III) and was poorly crystalline. In microcosms with strain RCH1 and hematite, Cr precipitates appeared to be concentrated in organic biofilms. Reaction between birnessite and the abiotically formed Cr(III) solids led to production of significant dissolved Cr(VI) compared to the no-birnessite controls. This pattern was not observed in the solids generated by microbial Cr(VI) reduction, possibly due to re-reduction of any Cr(VI) generated upon oxidation by birnessite by active bacteria or microbial enzymes. The results of this study suggest that Fe-Cr precipitates formed in groundwater remediation may remain stable only in the presence of active anaerobic microbial reduction. If exposed to environmentally common Mn oxides such as birnessite in the absence

of microbial activity, there is the potential for rapid (re)formation of dissolved Cr(VI) above regulatory levels.

1. Introduction

Anthropogenic contamination of ground water with toxic hexavalent chromium (Cr(VI)) has been reported in countries around the world and is due to waste emissions from industries such as electroplating and wood treatment,[1] leather tanning,[1,2] and chromite ore processing.[3,4] In-situ treatment of ground water contaminated with toxic Cr(VI) involves reduction to Cr(III) and subsequent immobilization as an insoluble Cr(III) precipitate (e.g., Dresel et al.[5] and references therein). The reducing agent for Cr(VI) can be an organic or inorganic electron donor in the case of microbially mediated Cr(VI) reduction (reviewed in Narayani and Shetty[6]), or, for abiotic Cr(VI) reduction, reactive mineral species containing Fe(II) or S(-II) such as FeS,[7,8] FeS_2,[9-12] green rust,[13-16] or clays.[17-19] Dissolved[20-22] or adsorbed[23] Fe(II), as well as reduced sulfur species[7,8,12,24] can also reduce Cr(VI) to Cr(III).

Because of the low solubilities, equivalent charges, and similar ionic radii of both Cr(III) and Fe(III), Cr(VI) reduction in the presence of iron minerals leads to formation of stable mixed Fe(III)-Cr(III) solid phases,[25] referred to hereafter as Fe-Cr precipitates or solids. The Fe source for such solids could include native Fe-bearing minerals such as clays and Fe(III) oxyhydroxides, or, in the case of abiotic Cr(VI) reduction by Fe(II) minerals, the Fe(III) that forms from oxidation of Fe(II) by Cr(VI).

A variety of manganese (Mn) oxides have been shown to oxidize Cr(III), including pyrolusite,[26] buserite,[27] δ-MnO_2,[28-30] manganite,[31] birnessite,[32-34] and colloidal Mn biooxides.[35] In addition, a column study conducted over four years established Mn oxides as the predominant oxidants for Cr(III) in soils.[36] The ability of Mn oxides to oxidize dissolved Cr(III) to Cr(VI) has also been confirmed in natural systems.[37-43] The rate of oxidation of mineral Cr(III) may be proportional to solubility,[39,42] since the electron transfer takes place between dissolved Cr(III)

and the Mn oxide surface.[39,44,45] Organic ligands have the potential to impact the solubility of Cr(III) solids and therefore the oxidation rate of Cr(III).[46]

The goal of any in situ remediation technology for Cr immobilization should be generation of the most insoluble Cr(III) precipitate possible. Since the solubility of mixed Fe-Cr precipitates is inversely proportional to the Fe:Cr ratio,[25] slower Cr oxidation is likely for precipitates with higher Fe:Cr ratios. More rapidly formed minerals may also be more soluble.[47] While others have demonstrated the oxidation of Cr(III) to Cr(VI) by Mn oxides, most studies have accomplished this by addition of dissolved Cr(III) to synthetic Mn oxides or to soils containing Mn minerals. Often, the solubility of Cr(III) in these studies is enhanced by carrying out the experiments at low pH. This approach does not accurately model the rate or extent of Cr(III) oxidation in realistic systems, which are controlled by the solubility of Cr(III) or mixed Fe-Cr minerals. While other studies have shown evidence for oxidation of Cr(III) minerals by Mn oxides,[39,42,48] a systematic investigation of the relationship between the processes of formation of Fe-Cr precipitates, their properties, and the rate and extent of their oxidation by Mn oxides is needed. The objective of this research was to fill this knowledge gap by preparing Fe-Cr precipitates under a range of relevant biogeochemical conditions, including both microbial and abiotic Cr(VI) reduction, characterizing them, and then testing their susceptibility to oxidation by the Mn oxide birnessite under realistic pH conditions. Our hypothesis was that the rate and extent of mobilization of Cr would be highest for those Fe-Cr solids formed most rapidly and for those with the lowest Fe:Cr ratios. The specific objectives of the research were to: (1) separately measure the rate of Cr(VI) reduction by redox active Fe(II) and S(-II) minerals and by a Cr(VI) reducing bacterial culture in the presence of Fe(III) minerals to serve as a Fe source for Fe-Cr precipitates; (2) characterize the size, structure, and composition of the resulting

solids; and (3) correlate solid properties with the rate and extent of subsequent Cr(VI) release upon exposure to birnessite.

2. Materials and Methods

All air sensitive samples were prepared in a Coy Products (Grass Lake, MI) anaerobic chamber with a catalytic oxygen removal system, and all experiments were performed under anoxic conditions, either in the chamber, or in sealed bottles. All aqueous solutions were sparged with nitrogen for 1 hour, then put in the anaerobic chamber unsealed at least overnight. All glassware was acid washed with 2 M nitric acid and autoclaved. The majority of chemical reagents were from Sigma-Aldrich (St. Louis, MO); exceptions are noted.

2.1. Culture Preparation

A culture of *Desulfovibrio vulgaris* strain RCH1,[49] a bacterium capable of Cr(VI) reduction that was previously isolated from the subsurface at the U. S. Department of Energy Hanford Site in Richland, Washington, was kindly provided by Dr. Romy Chakraborty at Lawrence Berkeley National Laboratory. It was grown anaerobically at 37 ^{o}C in lactate-sulfate medium, which contains 50 mM lactate, 25 mM sulfate, and 0.1% yeast extract as well as minerals, trace metals, and vitamins.[50] The 500 mL culture was harvested during log phase (OD600 of 0.8), washed and concentrated 2-3 times by centrifugation at 8,400-12,300 × g, and resuspended in 20 mL anaerobic 50 mM 4-(2-Hydroxyethyl)piperazine-1-ethanesulfonic acid (HEPES) buffer (pH 7.5) containing 5 mM $MgCl_2$, sealed in serum bottles, and kept on ice until use.

2.2. Mineral Preparation

Hematite was synthesized by forced hydrolysis of a Fe(III) salt solution (Schwertmann and Cornell[51] p. 122, Method 1). Goethite with approximately 9% substitution of Al for Fe ("Al-goethite") was prepared using the "alkaline Fe(III) system" method (Schwertmann and Cornell[51] pp. 86-88). Iron-rich nontronite (NAu-2) was purchased from The Clay Minerals Society (Chantilly, VA). The NAu-2 <0.15 μm fraction contains 37.85% Fe_2O_3,[52] and the majority of this Fe is in the +III oxidation state.[53] Clumps of NAu-2 were ground with a mortar and pestle, and the fraction that passed through a 100 mesh sieve was treated for carbonate removal with sodium acetate under ambient (not anaerobic) conditions as follows. Approximately 15 g was soaked in water for 24 h, then the supernatant was decanted. Next, 50 mL of 1 M sodium acetate (EMD), adjusted to pH 5.0 with glacial acetic acid (Fisher Scientific), was added, followed by occasional stirring in a water bath at 80 ^{o}C for 2 h. The mixture was then centrifuged and the process repeated until no bubbles of CO_2 formed in the solution. The treated NAu-2 was washed thoroughly and dispersed in water by sonication prior to use. NAu-2 treatment for carbonate removal was done to investigate the reactivity of the nontronite itself in Cr reduction.

For abiotic experiments, the Fe(III) in NAu-2 was reduced by sodium dithionite,[18,54] since dithionite reduction mimics the remediation approach used at several important Cr contaminated sites (e.g., Fruchter et al.[55]). Dithionite treatment may form very reactive adsorbed Fe(II) in addition to structural Fe(II).[56] Specifically, 200 mg NAu-2 was suspended in 40 mL of a buffer solution containing 0.22 M $NaHCO_3$ and 0.0083 M $Na_3C_6H_5O_7$ (sodium citrate) in a serum bottle inside the anaerobic chamber. Sodium dithionite was then added to the suspension at a final concentration of 0.1 M and the serum bottle was sealed and maintained at 70 ^{o}C for approximately 8 h. When the color of the mineral suspension changed completely from light brown to green-blue, the suspension was centrifuged and washed five times with N_2-sparged

water. No more than 4% of structural Fe was lost to solution when smectite underwent similar dithionite treatment.[54]

FeS was synthesized by precipitation using equal volumes of equal-concentration solutions of $FeCl_2 \cdot 4\ H_2O$ and $Na_2S \cdot 9\ H_2O$ inside the anaerobic chamber. The slurry was settled, decanted, and washed with N_2-sparged water four to five times prior to use.

2.3. Quantification of Cr

Dissolved Cr(VI) was quantified using a modified EPA Method 7199. Briefly, 105 μL of 6 N H_2SO_4 and 30 μL of 0.25% 1,5-diphenylcarbazide were added to 1.5 mL of aqueous sample after passing through a 0.2 μm syringe filter, followed by swirling and waiting approximately ten minutes for color development. The absorbance at 540 nm was then measured using a UV/vis spectrometer (Shimadzu UV1601). Total dissolved Cr was determined by atomic absorbance (AA) spectrometry by flame (above 0.2 μM) or furnace (below 0.2 μM) methods using a PerkinElmer AAnalyst 800. Aqueous samples were preserved before analysis by mixing with 10% trace-metals HCl at a 1:1 volume ratio. The concentration of Cr(III) was determined by the difference between total Cr and Cr(VI).

2.4. Cr(VI) reduction by bacteria or reduced minerals

For experiments set up for microbial reduction of Cr(VI), 500 mL of a solution containing 50 mM HEPES, 5 mM $MgCl_2$, 10 mM sodium lactate, and 1.3 g/L dry hematite, Al-goethite, or NAu-2 were added to a 1 L glass bottle modified by a glassblower (G. Finkenbeiner Inc., Waltham, MA) to have a serum bottle closure. The strain RCH1 culture was then added at a volume ratio of 1.1 part culture to 100 parts aqueous medium. Before adding Cr(VI), a drop of

the serum bottle contents was removed to prepare a grid for later transmission electron microscopy (TEM) analysis of the Fe(III) mineral before reaction with Cr(VI). To initiate Cr(VI) reduction, K_2CrO_4 (MP Biomedicals) was added at an initial Cr(VI) concentration of 50 μM. The serum bottle was then sealed and placed in a constant temperature chamber at 25±0.2 ^{o}C with constant stirring. Sampling was carried out at predetermined intervals until Cr(VI) was depleted and the concentration of dissolved Cr(III) was constant or below detection limits. Aqueous samples were withdrawn through the bottle septum with a disposable luer tip syringe fitted with a 20 gauge needle, and were immediately put on ice to stop or greatly slow the Cr(VI) reduction before analysis. Samples were then centrifuged at 7200 × g for five minutes and the supernatant filtered through a 0.2 μm syringe filter prior to measuring Cr(VI) and total Cr. At the end of the experiment, a second TEM grid was prepared for mineral characterization. The remaining solids were then removed by settling, and air-dried in a desiccator inside the anaerobic chamber and separate portions used for scanning electron microscopy (SEM), X-ray absorption spectroscopy (XAS), and reoxidation experiments with birnessite. One Cr(VI) reduction experiment with strain RCH1 and hematite was also done with a ten-fold lower loading of strain RCH1 (called "RCH1 slow") in order to yield a slower rate of Cr(VI) reduction and determine the impact of the Cr(VI) reduction rate, if any, on the properties of the resulting Fe-Cr precipitate. Finally, control microcosms that contained strain RCH1, with and without lactate, and with no Fe(III) minerals, were set up and the disappearance of Cr(VI) monitored. All experiments and controls were done in duplicate unless otherwise noted.

The experimental setup and procedures for the abiotic Cr(VI) reduction experiments by Fe(II) minerals were the same as those described above, except that strain RCH1 was not added, the initial Cr(VI) concentration was increased, and the mineral loading was decreased to

facilitate measurement of Cr(VI) reduction by the reduced minerals, which was very rapid. Abiotic experiments were done with either dithionite-reduced NAu-2 at a mass loading of 800 mg/L or with FeS at a mass loading of 31 mg/L. A much lower concentration of FeS was used since it reacted with Cr(VI) extremely rapidly; a higher FeS concentration would have led to a Cr(VI) reduction rate too rapid to measure using normal techniques. The target initial Cr(VI) concentration in the abiotic experiments was 200 μM.

The experiment with FeS was done in a tightly sealed 2 L screw cap glass bottle in order to recover sufficient solids for subsequent analyses. Two and three replicates were conducted for the experiments with dithionite-reduced NAu-2 and FeS, respectively.

2.5. Reaction of Fe-Cr precipitates with birnessite

Birnessite was synthesized using the method of McKenzie[57] and was characterized by X-ray diffraction as acid birnessite (not shown). Fe-Cr solids from all microbial and abiotic microcosms (i.e., the solids present in the Cr(VI) reduction experiments after Cr(VI) reduction was complete) were placed in an aqueous suspension of birnessite under anaerobic conditions, alongside controls containing no birnessite, for at least two weeks while monitoring dissolved Cr(VI) over time. These suspensions were buffered at pH 7.5 with 50 mM HEPES. HEPES was chosen as a buffer since it has been used for cultivation of *D. vulgaris* strain Hildenborough,[58] and since strict pH control was essential for the study of pH-sensitive redox transformations. HEPES also has a lower tendency for transition metal complexation than many biological buffers.[59] The mass concentration of the added Fe-Cr solid was 500 mg/L for all microbial experiments with strain RCH1, 800 mg/L for the abiotic experiment with dithionite-reduced NAu-2, and 31 mg/L for the abiotic experiment with FeS, while the concentration of birnessite

was 16 mg/L for all microbial experiments with strain RCH1 and 165 mg/L for both abiotic experiments. These conditions were chosen to ensure an excess of Mn (in birnessite) to Cr (in the Fe-Cr precipitates). Although we did not know the concentration of Cr that was incorporated into the Fe-Cr solids, we knew the maximum possible value of this concentration based on the concentrations of Fe(III) solid and Cr(VI) added to the Cr(VI) reduction experiments (Table ESI-1, column C). The concentration of Mn (in birnessite) was thus set to be at least approximately ten times this maximum possible concentration of Cr in the birnessite oxidation experiments (Table ESI-1, column I), to ensure an excess of Mn to Cr. The concentrations and proportions of Fe, Mn, and Cr in all experimental systems are outlined in detail in Table ESI-1.

2.6. Characterization of Fe-Cr precipitates

Both X-ray absorption near-edge structure (XANES) and extended X-ray absorption fine structure (EXAFS) spectroscopies were used to determine the oxidation state and structural environment of Cr in the Fe-Cr solids. Samples were mounted on a Teflon plate, and sealed with Kapton polyimide film to prevent moisture loss and oxidation while minimizing X-ray absorption. Samples were stored under anaerobic conditions during transport and while at the beamline until just immediately before mounting in a He-purged chamber. XAS data were collected on beamline 11-2 at the Stanford Synchrotron Radiation Lightsource (SSRL), running under dedicated conditions. Energy selection was accomplished with a Si(220) monochromator and higher-order harmonics were eliminated by detuning the monochromator ~60%. Absorption spectra were recorded by monitoring the Cr K_α fluorescence with a wide-angle ionization chamber[60] or a 30 element Ge solid-state detector array with Soller slits and a vanadium filter. Spectra (3-5 scans per sample) were collected at room temperature from -200 to +1000 eV about

the K_α-edge of Cr (5989 eV). Spectral data analysis was performed using the SIXPACK software program.[61] XAS scans were averaged, background-subtracted, normalized, and deglitched if necessary as described in detail previously.[62]

The relative percentage of Cr(VI) within the samples was calculated by dividing the height of the Cr(VI) pre-edge peak by the total atomic absorption, as the height of the Cr(VI) pre-edge peak is proportional to the concentration of Cr(VI), while the height of the total edge jump is proportional to the total amount of Cr.[7] A series of Fe(III):Cr(III) oxyhydroxides (3Fe:1Cr, 3Fe:2Cr, 1:Fe:1Cr, 2Fe:3Cr, 1Fe:3Cr) that were characterized previously[62] was used to construct a standard curve (R^2=0.99614) that was used to calculate the relative Cr(VI) concentration in the Fe-Cr solids.

For EXAFS analysis, the $\chi(k)$ spectra were k^3-weighted and analyzed using a k-range of 3-10 $Å^{-1}$. $\chi(k)k^3$ spectra were Fourier-transformed to produce the radial structure function in R-space (Å). The first shell peak in the Fourier transform was individually isolated and backtransformed (Fourier-filtered). A nonlinear least-squares procedure was used to fit both the Fourier-filtered and raw spectra by use of a theoretical reference XAS phase-shift and amplitude functions as described previously.[62] The coordination number (N), interatomic distance (R), and disorder (σ^2) were varied to minimize the residual.

Fe solids before and after reaction with Cr(VI) were deposited on 200-mesh holey carbon Cu TEM grids and characterized using a Zeiss NEON field emission SEM (10 kV), JEOL 2000FX TEM (LaB_6, 200 kV), and a JEOL 2010F field emission TEM (200 kV), all with energy-dispersive X-ray (EDS) detectors. TEM images were analyzed using Digital Micrograph (Gatan, Inc.), including the measurement of lattice fringe Fast Fourier Transforms with the DiffTools plugin.[63]

3. Results and Discussion

3.1. Cr(VI) reduction in microbial and abiotic microcosms

Cr(VI) disappeared relatively rapidly in all microcosms containing strain RCH1, but the extent of Cr(VI) removal in a no-lactate control was much less than when lactate was present (not shown). Chakraborty et al.[64,65] also reported the lactate dependent reduction of Cr(VI) by *D. vulgaris* strain RCH1 (first called strain HBLS[64]).

When Fe(III) minerals were present in microcosms containing strain RCH1 and lactate, dissolved Cr(VI) initially sharply decreased, followed by exponential decay, with larger and approximately equal initial losses for Al-goethite and hematite, and a smaller initial loss for NAu-2. (For brevity, results for RCH1/hematite are illustrated in Figure 1, and those RCH1/Al-goethite and RCH1/NAu-2, which were similar, are in Figures ESI-1 and ESI-2, respectively.) The sharp initial decline in Cr(VI) concentration is consistent with adsorption or partitioning to the solid phase. Increasing adsorption of negatively charged Cr(VI) (present primarily as CrO_4^{2-} at pH 7.5) in the order NAu-2 < Al-goethite ≈ hematite is consistent with the points of zero charge of these minerals (7.2 for NAu-2;[66] 8.1 for 10% Al-goethite;[67] and 8.8 for hematite[68]) that would result in a net negative surface charge for NAu-2, and hence less adsorption, and a net positive charge for Al-goethite and hematite, and thus more adsorption at the experimental pH of 7.5.

Differences in the rates of Cr(VI) removal after the initial loss were quantified by pseudo first order rate constants, calculated by non-linear regression using SigmaPlot 13.0 (Table 1). For microcosms containing minerals (except FeS), significantly better agreement between data and model, measured by the relative standard error, was found when excluding the time zero data

point in rate constant calculation, and designating the next measurement point as time zero. This was especially true for microcosms containing Al-goethite and hematite.

Calculated rate constants (Table 1) for Cr(VI) reduction by strain RCH1 indicate that hematite increased, NAu-2 decreased, and Al-goethite had a negligible effect on the rate of Cr(VI) removal, all compared to the RCH1/no mineral experiment. We considered several possible explanations for the rate enhancement by hematite. First, lactate could have reduced Cr(VI) in a process that was catalyzed by the hematite surface. This possibility, however, is not consistent with the comparatively slow rates for mineral catalyzed Cr(VI) reduction by organic acids.[69] Second, strain RCH1 could have reduced hematite to dissolved or adsorbed Fe(II), which then abiotically reduced Cr(VI). The evidence supporting this possibility is mixed. On the one hand, strain RCH1 is reported to reduce Fe(III)-NTA.[64,65] But on the other hand, *D. vulgaris* strain Hildenborough, found to be 99.9% similar to strain RCH1 by phylogenetic analysis,[64,65] showed only limited ability to reduce a poorly crystalline Fe(III) oxide in a process that did not appear to be linked with growth.[70] Also, while *D. vulgaris* strain Hildenborough can reduce dissolved Fe(III) in equilibrium with $Fe(OH)_3(s)$,[71] the low solubility of Fe(III) at neutral pH would make this an inefficient process. Nonetheless, since hematite is more soluble than goethite,[72] and aluminum substitution would tend to lower the solubility of goethite further,[72] faster Cr(VI) reduction in the presence of hematite versus Al-goethite is at least consistent with microbial Fe(III) reduction, since more soluble Fe(III) oxyhydroxides yield faster dissimilatory Fe reduction[73] and higher concentrations of dissolved Fe(III).

A third possible explanation for the higher rate constant for Cr(VI) reduction by strain RCH1 in the presence of hematite is toxicity reduction, possibly by adsorption and sequestration of significant Cr(VI) on the hematite surface. Priester et al.[74] studied Cr(VI) removal by

Pseudomonas putida biofilms and found that addition of hematite reduced the toxicity of Cr(VI) to the bacteria, as evidenced by higher cell yields and higher amounts of cellular protein and carbohydrate when hematite was present. It is not clear, however, why hematite would have such an effect on the rate of Cr(VI) reduction by strain RCH1, but not Al-goethite, which also appeared to initially adsorb significant amounts of Cr(VI) (Figure ESI-1).

The decrease in the rate of Cr(VI) reduction in the presence of NAu-2 (Table 1) might be explained by Al toxicity. Wong et al.[75] explained the inhibition of sulfate reduction by *D. vulgaris* strain Hildenborough by binding of Al^{+3} to cell components.[75] Unlike when NAu-2 was present, a similar decrease in the rate of Cr(VI) reduction was not seen in the RCH1/Al-goethite microcosm compared to the RCH1/no mineral microcosm (Table 1). Using solubility data for goethite reported in Schwertmann,[72] and assuming a lower solubility for Al-goethite compared to pure goethite[72] as well as congruous dissolution of Al and Fe in Al-substituted goethite,[76] the concentration of dissolved Al in equilibrium with Al-goethite is likely to be lower than that in the presence of NAu-2, which could explain why NAu-2 inhibited Cr(VI) reduction by strain RCH1, but Al-goethite did not.

Abiotic reduction of Cr(VI) by dithionite-reduced NAu-2 and FeS was very rapid (Figures ESI-3 and ESI-4, Table 1). For Cr(VI) reduction by FeS, the data fit equally well to a pseudo first order rate law regardless of whether the time zero data point was included, suggesting that adsorption of Cr(VI) was not significant for FeS, or that any adsorbed Cr(VI) was reduced faster than it was adsorbed. For dithionite-reduced NAu-2, however, the data fit a pseudo first order model significantly better when excluding the time zero data point, suggesting an initial loss of Cr(VI) to adsorption.

Recovery of dissolved Cr(III) was incomplete in all mineral-containing experiments (Figures 1, ESI-1, ESI-2, ESI-3, and ESI-4), indicating formation of mainly non-aqueous Cr(III) products. The transient accumulation of dissolved Cr(III) in some mineral microcosms containing strain RCH1 (e.g., hematite, Figure 1) indicates that the rate of Cr(VI) reduction to dissolved Cr(III) was faster than the rate of subsequent Cr(III) precipitation. To create conditions where the rate of Cr(VI) reduction might be slower, and thus slow the rate of Cr(III) precipitation and perhaps create a more ordered solid, a subsequent experiment was done with and without hematite and a ten-fold lower concentration of strain RCH1 ("RCH1 slow"). For Cr(VI) reduction by RCH1 slow/hematite, there was no significant accumulation of dissolved Cr(III) (not shown), meaning that the slower rate of Cr(VI) reduction (Table 1, Figure 2) likely slowed the rate of Cr(III) precipitation.

The proportion of Cr(VI) that disappeared at the very onset of the RCH1/hematite and RCH1 slow/hematite experiments was the same—about 50% (Figures 1 and 2)—which is consistent with an initial Cr(VI) loss due to adsorption to hematite (since the initial Cr(VI) concentrations and hematite masses were the same in both experiments). This initial loss was not seen in the RCH1 slow/no mineral experiments (Figure 2).

3.2. Characterization of Fe-Cr precipitates.

Due to site symmetry differences between Cr(VI) and Cr(III), the tetrahedral chromate ($Cr(VI)O_4^{2-}$) ion is observed as a pre-edge feature while octahedrally coordinated Cr(III) within oxyhydroxides is represented by the main edge feature (e.g., refs.[7,62,77]) of the absorption spectra. A strong Cr absorption edge with a peak position at ~6006 eV is consistent with the presence of Cr(III) within all the Fe-Cr precipitates, and similar to that for the mixed Fe(III):Cr(III)

oxyhydroxide standards (Figure 3A). The Fourier transforms of the k^3-weighted Cr EXAFS data for the solids are also similar to those for the mixed Fe(III):Cr(III) oxyhydroxide standards (Figure 3B). Further, least squares fitting of the first shell peak confirms that Cr is octahedrally coordinated (N = 5.5-5.6) with a Cr-O radial distance of 1.99-2.00 Å, which corresponds well with the structure of mixed Fe(III):Cr(III) oxyhydroxides (Cr-O = 2.00 Å; see ref.[62] for full structural refinement data).

While previous studies have shown the utility of relative peak intensities of different shells in the Fourier transform for determining the relative ratio of Cr(III) to Fe(III), glitches in high *k* data of the EXAFS spectra precluded such analysis for these samples. Yet, instead a subtle change is observed in the post-edge feature as a function of the relative Cr(III) content with the mixed Fe(III):Cr(III) oxyhydroxide standards (Figure 3A inset). Thus, while qualitative, this XAS post-edge line shape suggests a higher proportion of Cr in the Fe-Cr precipitate formed via Cr(VI) reduction by FeS compared to the others (Figure 3A). Consistent with this, SEM/EDS of this solid showed elevated Cr, increased O, and decreased S after reaction with Cr(VI) (Figures 4A and 4B), suggesting formation of a Fe-Cr hydroxide, also reported by Patterson et al.[7] (The oxygen detected in the unreacted FeS was likely from oxygen introduced to the sample when placing it in the SEM.) TEM analysis of FeS after reacting with Cr(VI) indicates a poorly crystalline, nearly amorphous material (Figure 4C). Although there were no distinct morphological changes in the reduced NAu-2 after reaction with Cr(VI) (not shown), like for FeS, elevated Cr was detected in the resulting Fe-Cr solid by EDS. The high Cr detected in the solids formed from Cr(VI) reduction by reduced NAu-2 and FeS is likely due to the higher proportion of Cr relative to Fe used in preparing the microcosms (Table ESI-1).

Solids from microcosms with strain RCH1 typically included only trace amounts of Cr by EDS (with Fe:Cr ratios typically > 10:1), and typically showed no distinct or consistent morphological changes by TEM, with the exception of those from the RCH1/hematite microcosm. Specifically, TEM/EDS analyses of the hematite surface after Cr(VI) reduction by strain RCH1 showed a possible organic film (Figure 5A) in which Cr rich, possible Fe:Cr hydroxide nanoparticles were observed alongside rhombic hematite particles (Figure 5B)). Such biofilms were not observed in solids from the RCH1 slow/hematite microcosms. Representative EDS spectra of the particles before reaction, after reaction but not in the film, and after reaction and in the film (Figure 5C) show a successive decrease in the Fe:Cr ratio, suggesting that Cr(III) in the RCH1/hematite system may have been concentrated in biofilms. Exposure of bacteria to toxic Cr(VI) can lead to increased production of extracellular polymeric substances (EPSs) that make up a significant component of biofilm mass.[74,78] Since dissolved Cr(III) is present primarily as the cation $Cr(OH)_2^+$ at the pH of these experiments (7.5), it would tend to form complexes with acidic EPS functional groups and accumulate on biofilm bacteria,[74] thus concentrating in biofilms.

In addition to observations of an organic film, there were distinct morphological differences in the hematite particles in the RCH1/hematite system before (Figures 6A-C) and after (Figures 6D-F) reaction with Cr(VI). After reaction, images show jagged edges and pitting (Figure 6D), as well as development of reaction rims or a non-continuous layer at the edges of some particles (Figure 6E-F), suggesting dissolution of hematite. However, Cr, if present, was not above detection limits in this layer. Again, these features were not observed in solids from the RCH1 slow/hematite microcosms.

Although the majority of solid phase Cr in the precipitates was in the +III oxidation state, solid phase Cr(VI) was also detected, as illustrated by a strong pre-edge feature in the Cr absorption spectra for all precipitates, except those formed via Cr(VI) reduction by FeS (Figure 3A). Using the ratio of the Cr(VI) pre-edge peak relative to the normalized jump height of the absorption spectra,[7] the relative concentration of Cr(VI) in the precipitates (i.e., Cr(VI)/Cr_{TOTAL}) ranged from 4 - 25% (Table 1). This proportion of Cr(VI) is lower than the amount believed to be initially lost to adsorption in some experiments (which was closer to 50% (Figures 1, 2, ESI-1, and ESI-3)), suggesting that some initially adsorbed Cr(VI) was subsequently reduced to Cr(III). The highest relative concentrations of Cr(VI) were from microcosms that contained hematite and Al-goethite (Table 1). Remarkably, this adsorbed or otherwise immobilized Cr(VI) remained associated with the solids long after dissolved Cr(VI) disappeared, since Cr(VI) reduction experiments were typically carried out for extended times before the solids were removed for XAS analysis. For example, the RCH1/hematite experiment shown in Figure 1 was continued for a total of 166 h, yet significant Cr(VI) was still present in the resulting precipitate after that time (Table 1), indicating its unavailability to microbial or abiotic reduction, and/or its stability when associated with the solid phase.

The relative concentrations of Cr(VI) in the precipitates (Table 1) are consistent with the trends for initial removal of Cr(VI) by adsorption discussed earlier, i.e., there was more Cr(VI) associated with hematite and Al-goethite compared to NAu-2, consistent with more Cr(VI) adsorption, and very little Cr(VI) in the precipitate generated by FeS, consistent with negligible adsorption. The relative concentrations of Cr(VI) in the solids were also very close for the RCH1/hematite and RCH1 slow/hematite experiments (24 and 21%, respectively), also consistent with initial loss of Cr(VI) by adsorption to hematite.

3.3 Reaction of Fe-Cr precipitates with birnessite.

Solids from each Cr(VI) reduction experiment were equilibrated in aqueous suspensions of birnessite, along with controls containing no birnessite, for at least two weeks. Prior studies have shown that Cr(III) oxidation by birnessite requires initial dissolution of the solid, followed by oxidation of dissolved Cr(III) at the manganese oxide surface.[39,44,45] All solids from microcosms that contained strain RCH1 and either hematite or Al-goethite showed no difference in trends of dissolved Cr(VI) versus time when exposed to birnessite compared to the no-birnessite controls. Profiles for RCH1/hematite, RCH1 slow/hematite, and RCH1/Al-goethite were very similar, so only the first is illustrated in Figure 7A for brevity and the remainder are shown in Figure ESI-5. Note that some of the concentrations shown in Figure 7 and ESI-5 are below the concentration range where the spectrophotometric analysis of Cr(VI) yielded a linear response (0.02-0.05 μM) and are therefore semi-quantitative. The uncertainties in these measurements are reflected in the relatively large error bars for the concentrations shown in Figures 7A and B and ESI-5. Thus, we focus this discussion on the differences in behavior for the systems with and without birnessite, rather than on individual Cr(VI) measurements.

Exposure of precipitates formed from strain RCH1 and either hematite or Al-goethite showed an initial increase in dissolved Cr(VI) before 100 h (Figures 7A and ESI-5), perhaps due to desorption, followed by a subsequent decrease to non-detection, perhaps due to direct or indirect microbial reduction. Although no active culture was added to either the samples containing birnessite or the no-birnessite controls, the solids were not sterilized or autoclaved after removal from the microbial cultures, and may have contained viable cells and/or enzymes capable of Cr(VI) reduction that were released upon cell lysis. The similar profiles of dissolved

Cr(VI) versus time in the solids produced in the RCH1 microcosms, regardless of whether birnessite was present, suggests that desorption, and not oxidation by birnessite, was responsible for the initial Cr(VI) release.

For the solids from the RCH1/NAu-2 microcosm, there was again no difference in the endpoint of dissolved Cr(VI) versus time for the experiment with and without birnessite (Figure 7B). But unlike the trend for the other microbially generated solids (Figures 7A and ESI-5), the concentration of Cr(VI) in the presence of the RCH1/NAu-2 precipitates did not decrease after an initial increase, perhaps due to lack of viable cells or reductase enzymes.

Unlike the trend with the microbially-generated solids, the precipitates produced in the abiotic Cr(VI) reduction microcosms showed a steady increase in concentration of Cr(VI) over time in the presence of birnessite, but not in the no-birnessite controls (Figures 7C and 7D). The rate of Cr(VI) release in these microcosms appeared to slow over the days of exposure to birnessite, perhaps due to adsorption of Mn^{+2} or other species to the birnessite surface,[42,48] or due to ripening of the birnessite structure to a less reactive form.[79] The most likely explanation for the distinct pattern in the abiotically (Figures 7C and 7D) and microbially (Figures 7A, 7B, and ESI-5) generated precipitates is lack of re-reduction of Cr(VI) in the experiments with the abiotically generated Fe-Cr solids, due to lack of viable microbial cells or enzymes. Numerous studies have shown that subsurface microbial activity and the availability of biodegradable organic carbon strongly influence the speciation of Cr.[36,80-83] In this study, EPS from biofilms may have provided biodegradable organic carbon that helped to keep Cr reduced in the microbially generated Fe-Cr precipitates. The fact that there was no Cr(VI) released from the FeS precipitate in the no-birnessite control indicates a lack of sorbed or easily releasable Cr(VI)

in this solid, consistent with the XAS results and the good fit of the data to a first order model that did not consider an initial loss to adsorption (Figure ESI-4).

The average rate of Cr(VI) release from the FeS-Cr precipitate upon exposure to birnessite during the period shown in Figure 7D was approximately 3 nM h^{-1}, at the high end of the range of rates for comparable pH values for chromite oxidation by birnessite[39] and similar to those reported for the more soluble fuchsite.[42] Because Cr oxidation rates are highly dependent upon mineral loadings,[39,42] no quantitative comparison between rates should be made, but the relatively high rate of Cr(VI) formation in the FeS-Cr precipitate may be due to its high Cr(III) solubility arising from its low Fe:Cr ratio (Table ESI-1, Figures 3A, 4A-B) or poorly crystalline structure (Figure 4C). The mean concentration of dissolved Cr(III) in equilibrium with this precipitate was estimated to be 0.2±0.1 μM (using measurements made at 19, 74, and 140 h in the Cr(VI) reduction experiment shown in Figure ESI-4 (not shown)), higher than for chromite (< 85 nM[39]), which helps to explain the relatively high rate of Cr(VI) generation upon exposure of the FeS-Cr precipitate to birnessite. Notably, the dissolved concentration of Cr(VI) after only 478 hours (20 days) of exposure to birnessite was equal to 1.2 μM (0.06 mg/L) (Figure 7D), above the World Health Organization (WHO) total Cr guideline of 0.05 mg/L and close to the current U.S. Maximum Contaminant (MCL) level of 0.1 mg/L. Longer term experiments are needed to quantify total Cr(VI) released from the abiotic precipitates in the presence of birnessite over time.

4. Environmental Implications

While Cr(VI) was initially "immobilized" by reduction and subsequent precipitation and, in some cases, adsorption, in microcosms containing both minerals and bacteria, there were

noticeable differences in the oxidation state, crystallinity, and Fe:Cr ratios of the resulting solid-phase Cr species that could ultimately affect the long and even near-term stability of the immobilized Cr. Significant Cr(VI) mobilization by birnessite was noted for two precipitates that were generated abiotically and when no bacteria were present, perhaps due to the absence of bacteria or enzymes capable of re-reducing any Cr(VI) that was formed by birnessite. For the Cr precipitate formed when FeS reduced Cr(VI), dissolved Cr(VI) reached a concentration above the WHO standard and close to the U.S. MCL within only 20 days of exposure to birnessite, even under strictly anaerobic conditions. And for the precipitate formed from Cr(VI) reduction by dithionite-reduced NAu-2, the concentration of dissolved Cr(VI) was not much lower after the same time. This suggests that in subsurface environments rich in naturally occurring Mn oxides such as birnessite, Cr immobilized in/by abiotic minerals will be stable only under conditions of anaerobic respiration. Although highly oxidized Mn(III,IV) oxides are unlikely to be stable under conditions of anaerobic microbial respiration, if such respiration is generated by addition of electron donors as part of a Cr(VI) remediation strategy, Cr(VI) could be mobilized if/when the donor addition stops and the site reverts to aerobic conditions.

Acknowledgements

Funding for this work was provided by the U. S. Department of Energy Subsurface Biogeochemical Research Program (grant DE-SC0006902). We thank Dr. Romy Chakraborty at Lawrence Berkeley National Lab for providing the culture of *D. vulgaris* strain RCH1, Jingling Hu and Preston Larson at the University of Oklahoma for help with laboratory and SEM measurements, respectively, and Yuanzhi Tang at Harvard University for preparing the Al-goethite. Part of this research was conducted at the Stanford Synchrotron Radiation Lightsource.

Use of the Stanford Synchrotron Radiation Lightsource, SLAC National Accelerator Laboratory, is supported by the U.S. Department of Energy, Office of Science, Office of Basic Energy Sciences under Contract No. DE-AC02-76SF00515. We thank the anonymous reviewers for careful review and insightful comments.

References

1. L. M. Calder, in *Chromium in the Natural and Human Environments*, ed. J. O. Nriagu, John Wiley and Sons, New York, 1988, vol. 20, ch. 8, pp. 215-265.
2. G. V. Iyer, Mastorakis, N. E., Proceedings of the IASME/WSEAS International Conference on Energy & Environmental Systems, Chalkida, Greece, 2006.
3. A. S. Hursthouse, *J Environ Monitor*, 2001, **3**, 49-60.
4. G. Stoecker, in *Elements and their Compounds in the Environment, 2nd Ed.*, ed. E. Merian, Anke, M., Ihnat, M., Stoeppler, M., Wiley-VCH, Weinheim, 2004, vol. 2: Metals and their Compounds, ch. 7, pp. 709-729.
5. P. E. Dresel, D. M. Wellman, K. J. Cantrell and M. J. Truex, *Environ Sci Technol*, 2011, **45**, 4207-4216.
6. M. Narayani and K. V. Shetty, *Crit Rev Env Sci Tec*, 2013, **43**, 955-1009.
7. R. R. Patterson, S. Fendorf and M. Fendorf, *Environ Sci Technol*, 1997, **31**, 2039-2044.
8. M. Mullet, S. Boursiquot and J. J. Ehrhardt, *Colloid Surface A*, 2004, **244**, 77-85.
9. A. I. Zouboulis, K. A. Kydros and K. A. Matis, *Water Res*, 1995, **29**, 1755-1760.
10. F. Demoisson, M. Mullet and B. Humbert, *Environ Sci Technol*, 2005, **39**, 8747-8752.
11. C. M. Chon, J. G. Kim and H. S. Moon, *Hydrol Process*, 2007, **21**, 1957-1967.
12. Y. T. Lin and C. P. Huang, *Sep Purif Technol*, 2008, **63**, 191-199.

13. S. Loyaux-Lawniczak, P. Refait, J. J. Ehrhardt, P. Lecomte and J. M. R. Genin, *Environ Sci Technol*, 2000, **34**, 438-443.

14. A. G. B. Williams and M. M. Scherer, *Environ Sci Technol*, 2001, **35**, 3488-3494.

15. W. J. Lee and B. Batchelor, *Environ Sci Technol*, 2003, **37**, 535-541.

16. D. L. Bond and S. Fendorf, *Environ Sci Technol*, 2003, **37**, 2750-2757.

17. M. F. Brigatti, G. Franchini, C. Lugli, L. Medici, L. Poppi and E. Turci, *Appl Geochem*, 2000, **15**, 1307-1316.

18. R. W. Taylor, S. Y. Shen, W. F. Bleam and S. I. Tu, *Clay Clay Miner*, 2000, **48**, 648-654.

19. S. Loyaux-Lawniczak, P. Lecomte and J. J. Ehrhardt, *Environ Sci Technol*, 2001, **35**, 1350-1357.

20. D. L. Sedlak and P. G. Chan, *Geochim Cosmochim Ac*, 1997, **61**, 2185-2192.

21. L. E. Eary and D. Rai, *Environ Sci Technol*, 1988, **22**, 972-977.

22. M. Pettine, L. D'Ottone, L. Campanella, F. J. Millero and R. Passino, *Geochim Cosmochim Ac*, 1998, **62**, 1509-1519.

23. I. J. Buerge and S. J. Hug, *Environ Sci Technol*, 1999, **33**, 4285-4291.

24. M. Pettine, F. J. Millero and R. Passino, *Mar Chem*, 1994, **46**, 335-344.

25. B. M. Sass and D. Rai, *Inorg Chem*, 1987, **26**, 2228-2232.

26. L. E. Eary and D. Rai, *Environ Sci Technol*, 1987, **21**, 1187-1193.

27. E. Silvester, L. Charlet and A. Manceau, *J Phys Chem-Us*, 1995, **99**, 16662-16669.

28. S. E. Fendorf, M. Fendorf, D. L. Sparks and R. Gronsky, *J Colloid Interf Sci*, 1992, **153**, 37-54.

29. S. E. Fendorf and R. J. Zasoski, *Environ Sci Technol*, 1992, **26**, 79-85.

30. P. S. Nico and R. J. Zasoski, *Environ Sci Technol*, 2000, **34**, 3363-3367.

31. C. A. Johnson and A. G. Xyla, *Geochim Cosmochim Ac*, 1991, **55**, 2861-2866.

32. D. Banerjee and H. W. Nesbitt, *Geochim Cosmochim Ac*, 1999, **63**, 1671-1687.

33. J. G. Kim, J. B. Dixon, C. C. Chusuei and Y. J. Deng, *Soil Sci Soc Am J*, 2002, **66**, 306-315.

34. G. Landrot, M. Ginder-Vogel, K. Livi, J. P. Fitts and D. L. Sparks, *Environ Sci Technol*, 2012, **46**, 11594-11600.

35. K. J. Murray and B. M. Tebo, *Environ Sci Technol*, 2007, **41**, 528-533.

36. T. K. Tokunaga, J. Wan, A. Lanzirotti, S. R. Sutton, M. Newville and W. Rao, *Environ Sci Technol*, 2007, **41**, 4326-4331.

37. R. Bartlett and B. James, *J Environ Qual*, 1979, **8**, 31-35.

38. M. C. Amacher and D. E. Baker, *Redox reactions involving chromium, plutonium, and manganese in soils. Final report for the period 1 July 1978 to 30 September 1981, prepared for the U.S. Department of Energy under contract DE-AS08-77DP04515. Also submitted by M.S. Amacher as a thesis in soil chemistry for PhD. Degree, August 1981*, Pennsylvania State University, 1982.

39. C. Oze, D. K. Bird and S. Fendorf, *P Natl Acad Sci USA*, 2007, **104**, 6544-6549.

40. D. Fandeur, F. Juillot, G. Morin, L. Olivi, A. Cognigni, S. M. Webb, J. P. Ambrosi, E. Fritsch, F. Guyot and G. E. Brown, *Environ Sci Technol*, 2009, **43**, 7384-7390.

41. C. T. Mills, J. M. Morrison, M. B. Goldhaber and K. J. Ellefsen, *Appl Geochem*, 2011, **26**, 1488-1501.

42. A. U. Rajapaksha, M. Vithanage, Y. S. Ok and C. Oze, *Environ Sci Technol*, 2013, **47**, 9722-9729.

43. A. R. Wadhawan, A. T. Stone and E. J. Bouwer, *Environ Sci Technol*, 2013, **47**, 8220-

8228.

44. R. Milacic and J. Stupar, *Environ Sci Technol*, 1995, **29**, 506-514.

45. R. M. Weaver, M. F. Hochella and E. S. Ilton, *Geochim Cosmochim Ac*, 2002, **66**, 4119-4132.

46. R. F. Carbonaro and A. T. Stone, *Environ Chem*, 2015, **12**, 33-51.

47. A. C. Cismasu, F. M. Michel, J. F. Stebbins, C. Levard and G. E. Brown, *Geochim Cosmochim Ac*, 2012, **92**, 275-291.

48. R. A. Dai, J. Liu, C. Y. Yu, R. Sun, Y. Q. Lan and J. D. Mao, *Chemosphere*, 2009, **76**, 536-541.

49. R. Chakraborty, Desulfovibrio vulgaris RCH1, complete genome, GenBank: CP002297.1, 2011, http://www.ncbi.nlm.nih.gov/nuccore/CP002297.1).

50. J. L. Groh, Q. W. Luo, J. D. Ballard and L. R. Krumholz, *Appl Environ Microb*, 2005, **71**, 7064-7074.

51. U. Schwertmann and R. M. Cornell, *Iron oxides in the laboratory: preparation and characterization*, Wiley-VCH, Weinheim ; New York, 2nd completely rev. and extended edn., 2000.

52. J. L. Keeling, M. D. Raven and W. P. Gates, *Clay Clay Miner*, 2000, **48**, 537-548.

53. D. P. Jaisi, R. K. Kukkadapu, D. D. Eberl and H. L. Dong, *Geochim Cosmochim Ac*, 2005, **69**, 5429-5440.

54. J. W. Stucki, D. C. Golden and C. B. Roth, *Clay Clay Miner*, 1984, **32**, 191-197.

55. J. S. Fruchter, C. R. Cole, M. D. Williams, V. R. Vermeul, J. E. Amonette, J. E. Szecsody, J. D. Istok and M. D. Humphrey, *Ground Water Monit R*, 2000, **20**, 66-77.

56. J. E. Szecsody, J. S. Fruchter, M. D. Williams, V. R. Vermeul and D. Sklarew, *Environ*

Sci Technol, 2004, **38**, 4656-4663.

57. R. M. McKenzie, *Mineral Mag*, 1971, **38**, 493-502.

58. M. J. Wilkins, D. W. Hoyt, M. J. Marshall, P. A. Alderson, A. E. Plymale, L. M. Markillie, A. E. Tucker, E. D. Walter, B. E. Linggi, A. C. Dohnalkova and R. C. Taylor, *Front Microbiol*, 2014, **5**, 507.

59. N. E. Good, G. D. Winget, W. Winter, T. N. Connolly, S. Izawa and R. M. M. Singh, *Biochemistry*, 1966, **5**, 467-477.

60. F. W. Lytle, R. B. Greegor, D. R. Sandstrom, E. C. Marques, J. Wong, C. L. Spiro, G. P. Huffman and F. E. Huggins, *Nucl Instrum Meth A*, 1984, **226**, 542-548.

61. S. M. Webb, *Phys Scripta*, 2005, **T115**, 1011-1014.

62. C. M. Hansel, B. W. Wielinga and S. R. Fendorf, *Geochim Cosmochim Ac*, 2003, **67**, 401-412.

63. D. R. G. Mitchell, *Microsc Res Techniq*, 2008, **71**, 588-593.

64. R. Chakraborty, E. L. Brodie, J. Van Nostrand, J. Zhou and T. C. Hazen, Presentation at the 108th General Meeting of the American Society for Microbiology, Boston, MA, 2008.

65. R. Chakraborty, Brodie, E. L., B. Faybishenko, B., Piceno, Y. M., Tom, L., Chaudhuri, S., Beller, H. R., Liu, J., Torok, T., Joyner, D. C., Newcomer, D. R., Long, P. E., Andersen, G. L., Hazen, T. C., presented in part at the American Society for Microbiology 110th General Meeting, San Diego, CA, 5/23/10-5/27/10, 2010.

66. D. P. Jaisi, C. X. Liu, H. L. Dong, R. E. Blake and J. B. Fein, *Geochim Cosmochim Ac*, 2008, **72**, 5361-5371.

67. M. G. Ma, H. Y. Gao, Y. B. Sun and M. S. Huang, *J Mol Liq*, 2015, **201**, 30-35.

68. A. S. Madden, M. F. Hochella and T. P. Luxton, *Geochim Cosmochim Ac*, 2006, **70**, 4095-4104.

69. B. L. Deng and A. T. Stone, *Environ Sci Technol*, 1996, **30**, 2484-2494.

70. D. R. Lovley, E. E. Roden, E. J. P. Phillips and J. C. Woodward, *Mar Geol*, 1993, **113**, 41-53.

71. D. A. Elias, J. M. Suflita, M. J. McInerney and L. R. Krumholz, *Appl Environ Microb*, 2004, **70**, 413-420.

72. U. Schwertmann, *Plant Soil*, 1991, **130**, 1-25.

73. S. Bonneville, T. Behrends and P. Van Cappellen, *Geochim Cosmochim Ac*, 2009, **73**, 5273-5282.

74. J. H. Priester, S. G. Olson, S. M. Webb, M. P. Neu, L. E. Hersman and P. A. Holden, *Appl Environ Microb*, 2006, **72**, 1988-1996.

75. D. Wong, J. M. Suflita, J. P. McKinley and L. R. Krumholz, *Microbial Ecol*, 2004, **47**, 80-86.

76. E. B. Ekstrom, D. R. Learman, A. S. Madden and C. M. Hansel, *Geochim Cosmochim Ac*, 2010, **74**, 7086-7099.

77. M. L. Peterson, G. E. Brown, G. A. Parks and C. L. Stein, *Geochim Cosmochim Ac*, 1997, **61**, 3399-3412.

78. S. F. Aquino and D. C. Stuckey, *Water Res*, 2004, **38**, 255-266.

79. Y. Z. Tang, S. M. Webb, E. R. Estes and C. M. Hansel, *Environ Sci-Proc Imp*, 2014, **16**, 2127-2136.

80. B. R. James, J. C. Petura, R. J. Vitale and G. R. Mussoline, *J Soil Contam*, 1997, **6**, 569-580.

81. T. Makino, K. Kamewada, T. Hatta, Y. Takahashi and Y. Sakurai, *J Geochem Explor*, 1998, **64**, 435-441.

82. T. Becquer, C. Quantin, M. Sicot and J. P. Boudot, *Sci Total Environ*, 2003, **301**, 251-261.

83. B. Bohm and W. R. Fischer, *J Plant Nutr Soil Sc*, 2004, **167**, 22-23.

Table 1. Pseudo first order rate constants (k_{obs}) for Cr(VI) removal and relative concentrations of Cr(VI) in the Fe-Cr precipitates. Uncertainties in k_{obs} values are standard errors. The concentration at time zero was not included in rate constant calculations, except where noted. All microcosms for which data are reported here contained lactate.

Microcosm condition	**k_{obs} (h^{-1})**	**Cr(VI)/Cr_{TOT} (%)**
RCH1/no minerals	0.56±0.07 (t=0 included)	Not applicable
RCH1/Hematite	1.49±0.05	24
RCH1/Al-goethite	0.45±0.02	25
RCH1/NAu-2	0.177±0.006	11
RCH1 slow/No minerals	$(7.0\pm0.6)\times10^{-3}$ (t=0 included)	Not applicable
RCH1 slow/Hematite	$(6\pm1)\times10^{-3}$	21
Dithionite-reduced NAu-2	0.75±0.06	10
FeS	8.2±0.8 (t=0 included)	4

Figure 1

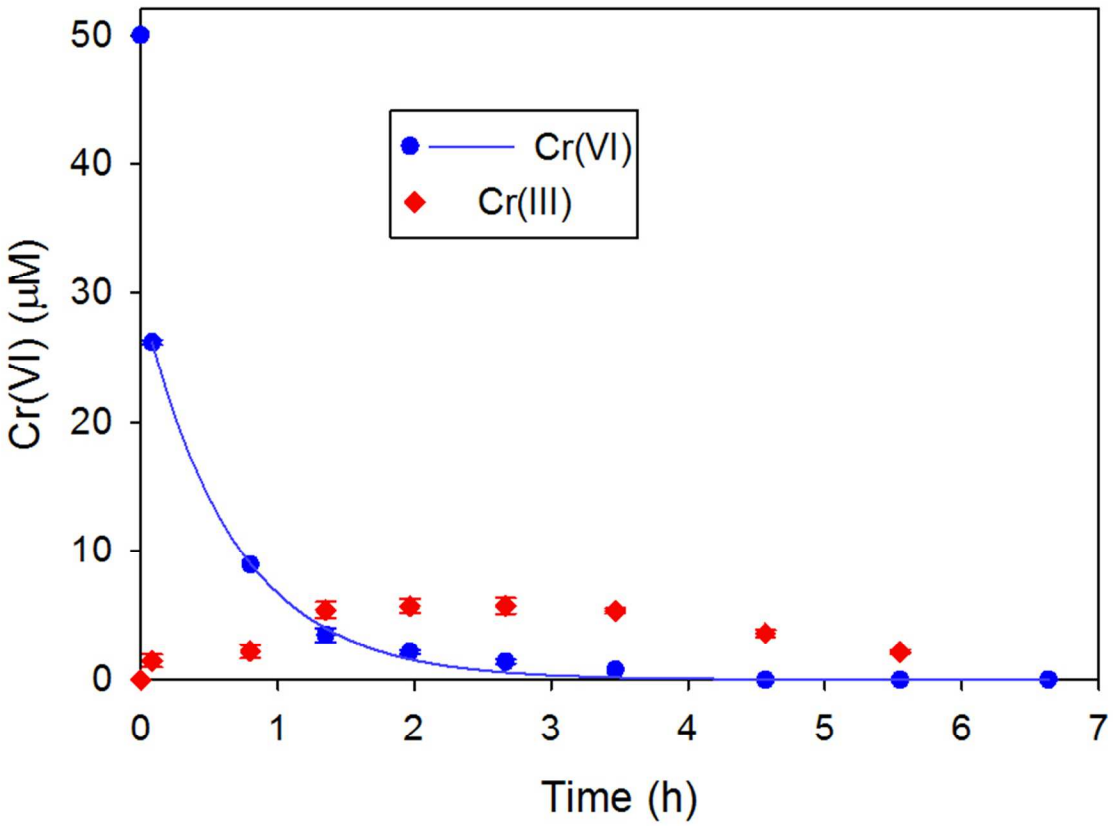

Figure 1. Concentrations of dissolved Cr(VI) and Cr(III) versus time in the RCH1/hematite microcosms. Error bars on symbols are the standard error of mean measurements from duplicate microcosms. The line shows the data fit to a pseudo first order rate law.

Figure 2

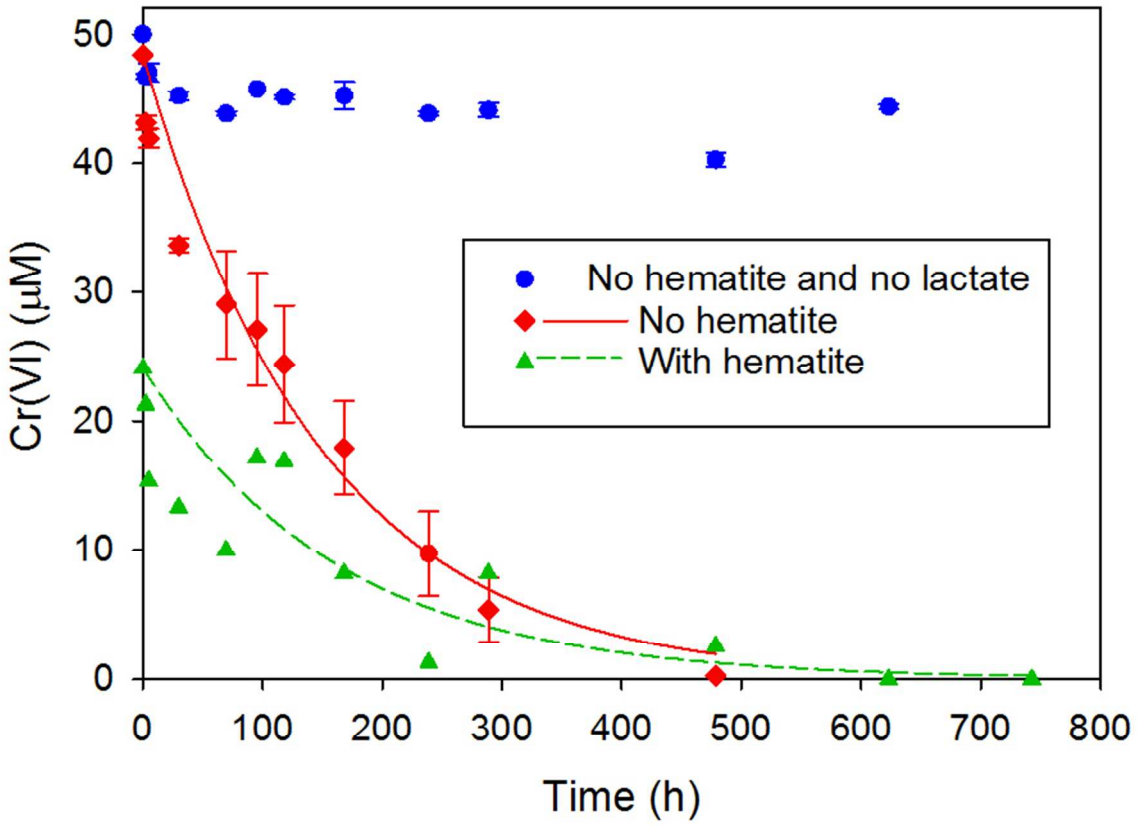

Figure 2. Concentration of dissolved Cr(VI) versus time in the RCH1 slow microcosms, with and without hematite. All microcosms contained lactate unless otherwise noted. Error bars are the standard error of the mean for measurements from duplicate microcosms, except that results for only one microcosm (no replicates) is shown for the experiment with hematite because there was no Cr(VI) reduction in the second microcosm. Lines show fit of the data to a pseudo first order rate law.

Figure 3

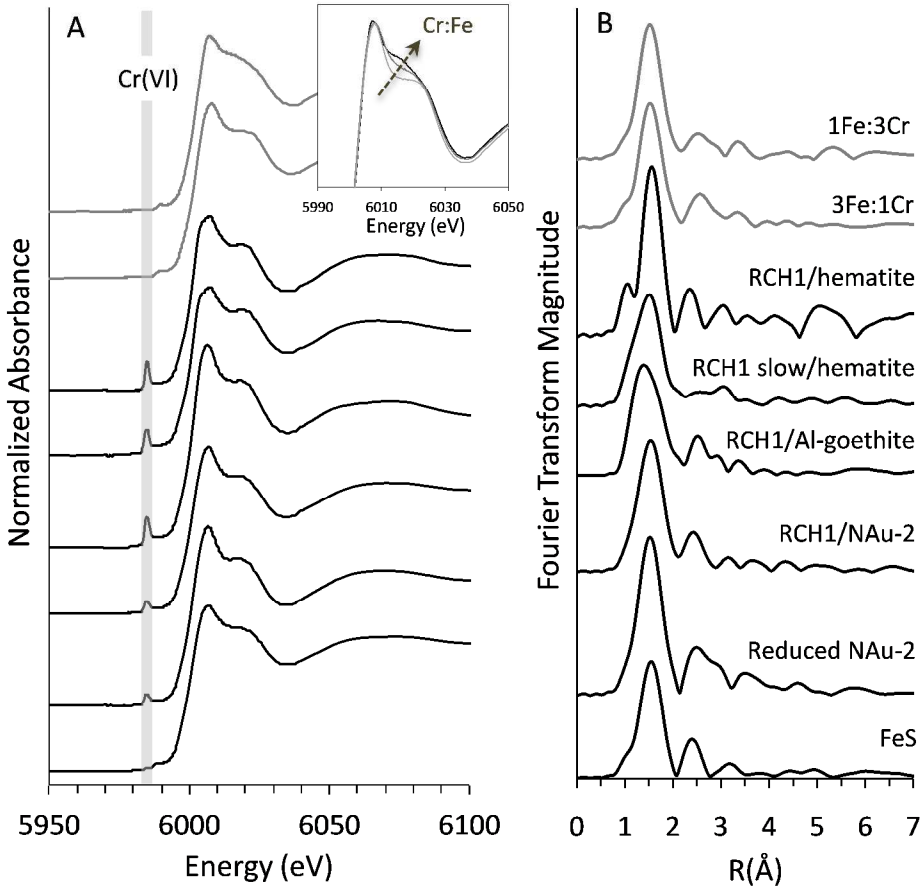

Figure 3. (A) Normalized Cr absorption spectra with the pre-edge Cr(VI) feature highlighted in gray. Inset illustrates a subtle, yet consistent, shift in the post-edge absorption spectra as a function of the ratio of Cr to Fe. (B) Fourier transforms of Cr K-edge EXAFS spectra for two end-member Fe(III):Cr(III) oxyhydroxide standards (gray, top two spectra) and Fe-Cr precipitates formed under the various conditions (black, bottom six spectra) as shown in (A).

Figure 4

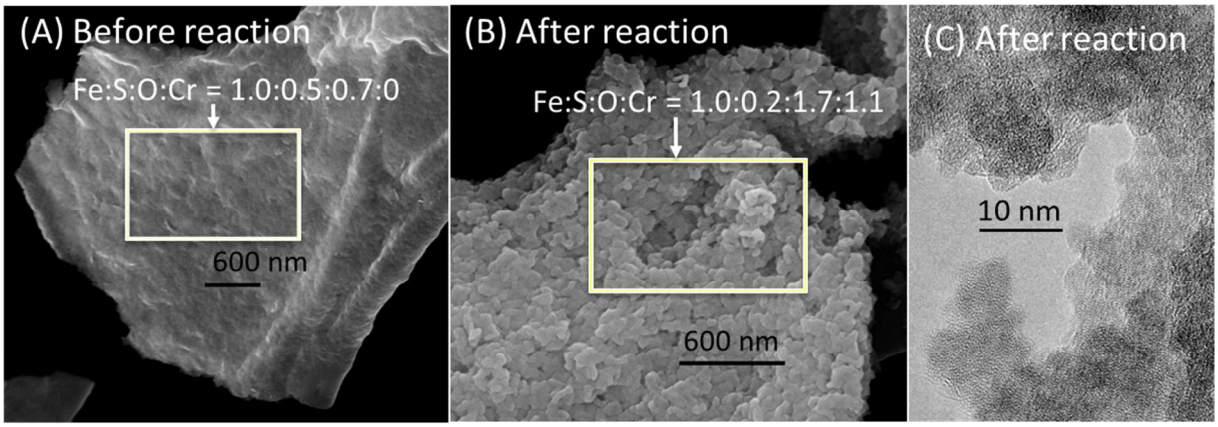

Figure 4. SEM (A, B) and TEM (C) images and EDS results for FeS (A) before and (B, C) after reaction with Cr(VI).

Figure 5

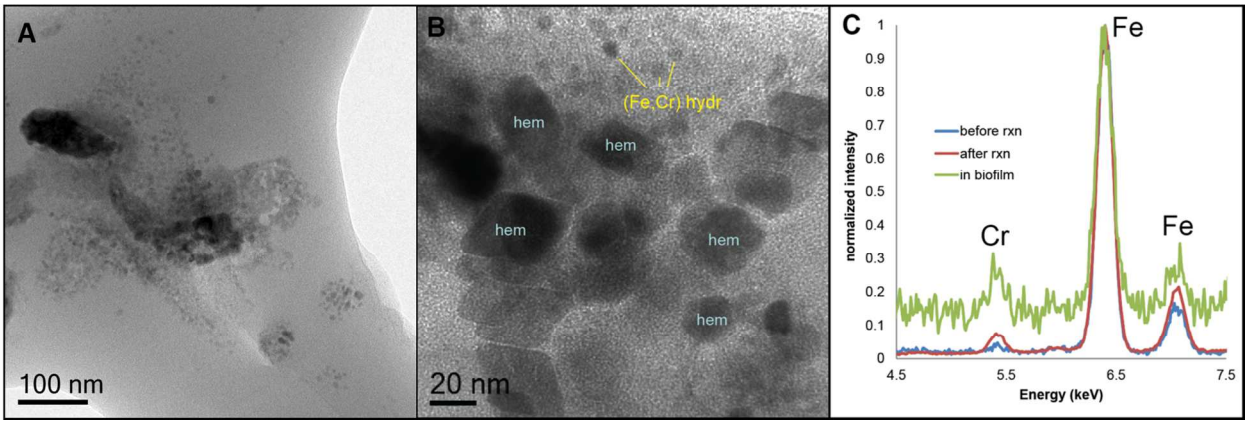

Figure 5. TEM images and EDS spectra of solids from the RCH1/hematite microcosm. (A) Film with elevated Cr (EDS results not shown), (B) 30-40 nm diameter hematite (some with rhombic morphology, others appearing more rounded in this view, presumably due to dissolution) distinguished from much smaller Cr-rich particles, (C) Representative EDS spectra.

Figure 6

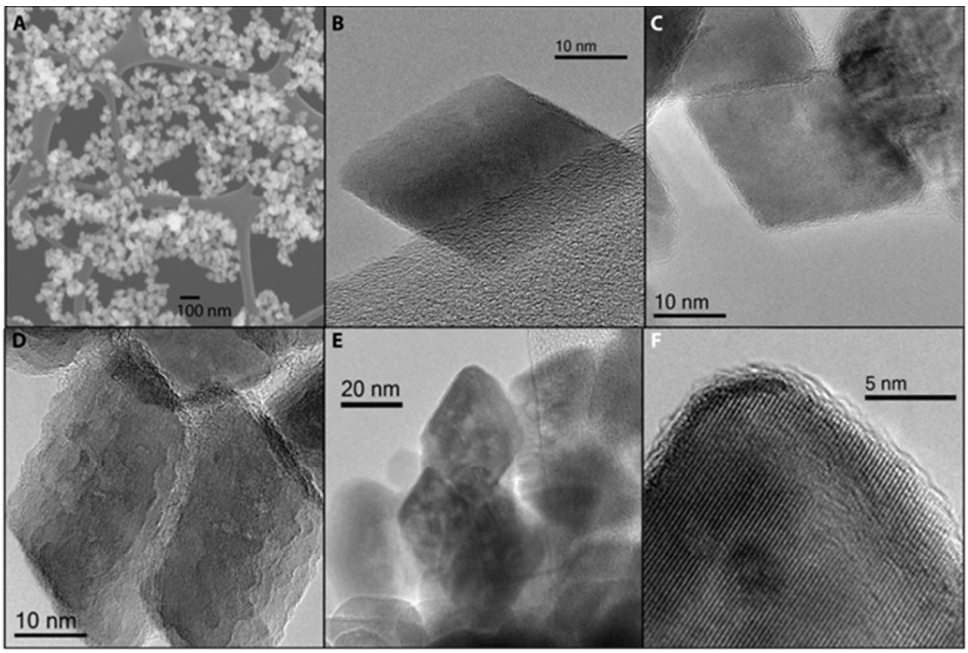

Figure 6. Solids from the RCH1/hematite microcosm before and after reaction with Cr(VI). (A) SEM and (B, C) TEM/HRTEM images of hematite before reaction; (D-F) TEM/HRTEM images of hematite after reaction.

Figure 7

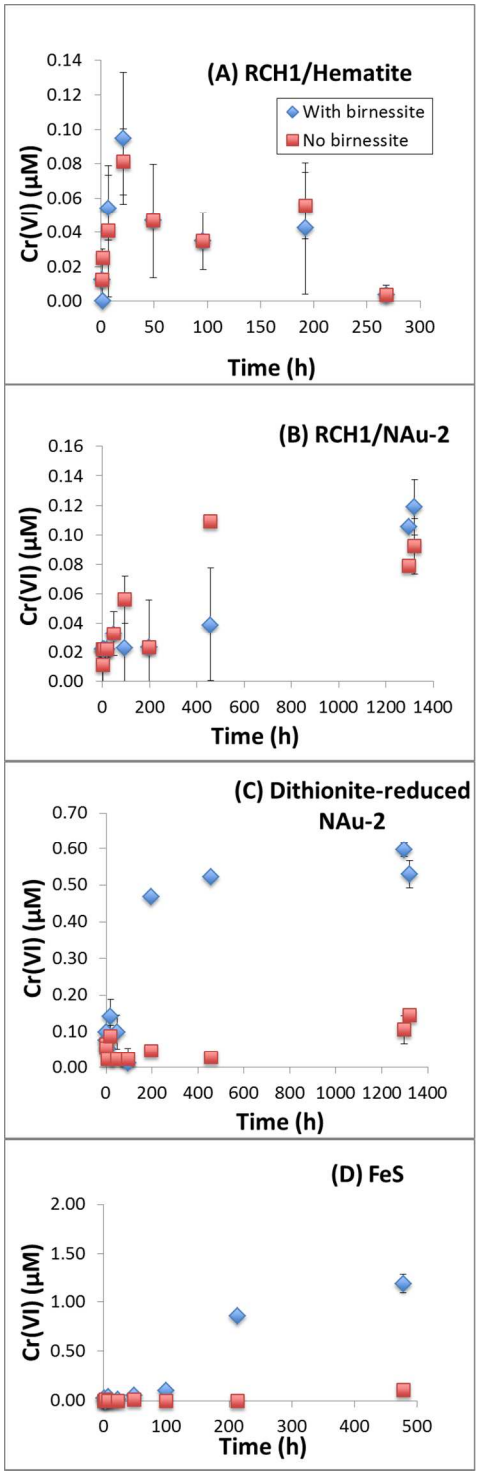

Figure 7. Cr(VI) versus time in precipitates exposed to birnessite.